Quantum Virial Coefficients of Molecular Nitrogen

Ramachandran Subramanian, Andrew J. Schultz, and David A. Kofke*

Department of Chemical and Biological Engineering,

University at Buffalo, The State University of New York,

Buffalo, New York 14260-4200, USA

(Dated: January 14, 2017)

Abstract

We report virial coefficients up to third order in density for molecular nitrogen, investigating 103 temperatures in the range [15 K, 3000 K]. All calculations are based on an *ab initio*-based potential taken from the literature. Path integral Monte Carlo (PIMC) is applied to account for nuclear quantum effects, and these results are compared to a more approximate but faster semiclassical treatment. Additionally, we examine a PIMC approach that employs semiclassical beads for the path-integral images, but find that it offers marginal advantage. A recently developed orientation sampling algorithm is used in conjunction with Mayer sampling to compute precise virial coefficients. We find that, within the precision of our calculations of the second-order coefficient (B_2), semiclassical methods are adequate for temperatures greater than 250 K, and are needed to correct classical behavior for temperatures as high as 800 K. For the third-order coefficient (B_3), the semiclassical methods are adequate above 150 K, and are required up to the highest temperature examined (3000 K) in order to correct the classical treatment within the precision of the calculations. However, three-body contributions to the potential are much more significant than nuclear quantum effects for evaluation of B_3.

Keywords: Quantum virial coefficients; nitrogen; Path Integral Monte Carlo

*Electronic address: kofke@buffalo.edu

I. INTRODUCTION

A. Virial coefficients

The virial equation of state describes the pressure p in terms of its deviation from the ideal gas model as a power series expansion in density ρ:

$$\frac{p}{\rho k_{\mathrm{B}} T} = 1 + B_2(T)\rho + B_3(T)\rho^2 + \ldots \tag{1}$$

where k_B is the Boltzmann constant and T the temperature. The coefficients of Eq. (1), $B_N(T)$ are called the virial coefficients and they depend only on the temperature and N-body interactions of the system [1–3]. By summing to the pressure, the virial coefficients provide a link between various interactions that occur at the microscopic level and a macroscopic observable. This unique feature makes the virial coefficients ideal candidates for performing accuracy checks of N-body interaction potentials or potential energy surfaces (PESs). Given a PES, one can perform this check by computing the virial coefficients via Monte Carlo (MC) integration or (for small N) numerical quadrature and comparing them with those obtained experimentally. Tuning the parameters of the PES to better suit experimental virial coefficient data and thereby obtaining a better quality PES is a common practice [4–9].

Given a PES defined in terms of an additive pair potential $U_2(\mathbf{r})$, the classical expressions for B_2 and B_3 can be written as integrals of Mayer f-functions as follows [3, 10]:

$$\begin{aligned} B_2(T) &= -\frac{1}{2}\int d1\ f(0,1), \\ B_3(T) &= -\frac{1}{3}\int\int d1\ d2\ f(0,1)\ f(0,2)\ f(1,2). \end{aligned} \tag{2}$$

where $f(0,1) = \Big(\exp\big[-\beta U_2(\mathbf{r})\big] - 1\Big)$ and indices '1' and '2' denote the position and orientational degrees of freedom of molecules 1 and 2, respectively, with respect to molecule '0' at the origin; also $\beta = 1/(k_{\mathrm{B}}T)$.

The number of integrals in Eq. (2) grows exponentially with increasing order of the virial coefficients and MC simulations or numerical techniques are needed [10]. The functional form of $U_2(\mathbf{r})$ adds further variation to the computational complexity of the calculation. For extremely simple potentials like hard spheres, up to fourth-order virial coefficients may be calculated analytically [10]. For more complicated potentials, stochastic methods such as

the VEGAS [11] algorithm or Mayer sampling Monte Carlo [12] have been used to evaluate virial coefficients.

One would expect a PES based on high-quality *ab initio* calculations to yield virial coefficients that are in better agreement with experimentally determined values, as compared to empirical potentials describing the same system. Empirical potentials incorporate multibody effects and other complications in an effective pairwise potential, which is therefore not describing the true intermolecular interactions; this inadequacy is highlighted in the calculation of the virial coefficients. However, *ab initio* PES calculations invoke the Born-Oppenheimer approximation, leading to the neglect of nuclear quantum effects which become increasingly important at low temperatures, particularly for low-mass atoms. Consequently for conditions where these effects are significant, one has to explicitly include them in virial coefficient calculations to obtain accurate results — e.g. nuclear quantum effects amount to 15% of the second virial coefficient of water vapor at 300 K [13, 14].

Virial coefficients evaluated without any such modification are known as classical virial coefficients. The classical values may be corrected perturbatively, and several ways have been established to do this (see Sec. II A). Application of such methods yields what are known as semiclassical virial coefficients. These values will be accurate to lower temperatures than classical values, but for sufficiently low temperature they too become inaccurate. The path integral Monte Carlo (PIMC) method provides a route to incorporate nuclear quantum effects that is more rigorous. In effect, it represents the positions of an atom as a closed ring of "beads". Adjacent beads experience a harmonic spring-like interaction which is characterized by a spring constant that is dependent on the mass of the atom, the temperature, and the discretization parameter (number of beads in the ring, P). The interaction energy is defined as the average of the intermolecular potential energy due to corresponding beads in each ring representing the other atoms in the system. Further detail is given in Sec. II B. Virial coefficients evaluated using the PIMC method to include nuclear quantum effects are known as (fully) quantum virial coefficients.

Fully quantum virial coefficients of helium-3 and helium-4 have been computed for temperatures from 2.6 K to 10,000 K, including exchange contributions where needed (exchange becomes relevant at much lower temperatures than other nuclear quantum effects, again depending on the atom mass) [15–20]. The complexity of such calculations, involving just monatomic molecules, is greatly reduced by the lack of rotational and vibrational degrees of

freedom. Multiatomics can be treated using a rigid-rotor approximation, and PIMC methods can be developed by invoking the conventional quantum-mechanical apparatus for describing such a system [21, 22]. In this approach, the path-integral "beads" possess an orientation as well as a position, and the interaction between adjacent beads includes a function of their relative orientation summed over rotational quantum numbers, as well as the harmonic contribution in their separation. An effective means to introduce intramolecular flexibility in this framework is to allow the geometry to be temperature dependent but otherwise rigid [23]. It has been applied to calculate virial coefficients of H_2 and its different isotopes, using both rigid and flexible *ab initio* PESs [21, 23–25]. An alternative way to approach PIMC for multiatomics is to focus on the atoms, treating each as its own quantum object with its own path-integral ring representation. Then intramolecular and intermolecular interactions are treated on the same footing (although the greater strength of the former requires some special handling, particularly for the rigid-molecule limit), path-integral beads again possess no orientation, and all bead-bead interactions are harmonic. This atom-focused approach arguably has some advantage in simplicity, requiring no sums over rotational quantum numbers, and it extends more naturally to flexible molecules. It has been applied to rigid and flexible models for H_2 [25, 26].

Regardless of the manner in which rotational nuclear quantum effects are expressed, there remains some choice in how to sample the orientations of the ring of path-integral images of each molecule (we use "image" to refer to the molecule in a path-integral ring, be it an oriented bead or a single path-integral time-slice of all the molecule's atoms). One option is to conduct MC rotation and displacement trials of each image [27]. This approach becomes very inefficient with increasing P, as adjacent images become more tightly coupled and of course larger in number. Garberoglio and Johnson introduced a hybrid MC technique employing a multiple-timestep molecular dynamics algorithm to generate new configurations of all images for a molecule [22, 25]. The most appealing approach is one in which the orientations can be sampled directly from the governing single-molecule distribution. This can be done exactly for the position coordinates in the ring, regrowing the entire ring in a single trial, but it can be accomplished only approximately for the orientations. We recently proposed an approach for diatomics based on this idea [26], and demonstrated its application for calculation of B_2 for H_2. We apply the algorithm again here for calculating B_2 and B_3 of molecular nitrogen and report new quantum virial coefficient data that are currently unavailable in literature.

We note that intermolecular as well as intramolecular exchange effects are neglected as part of this study.

In the next subsection we review recent advances in *ab initio* calculations and PESs related to nitrogen.

B. Nitrogen

Berns and van der Avoird [28] reported one of the first *ab initio* PES (BvdA) for the nitrogen ($N_2 - N_2$) dimer including first-order exchange, short-range electrostatic contributions and long-range data of Mulder et al. [29]. They developed two analytic representations of their calculations: 1) a spherical harmonic expansion and 2) a two-site point-charge model with a shifted-force center. An accurate description of the region near the van der Waals minimum was one of the primary goals of their work. The BvdA potential was used to study crystal structure properties [30] and transport properties [31]. Whereas the long-range interaction calculations performed by Mulder et al. [29] were obtained using an uncoupled Hartree-Fock (HF) method, Visser et al. [32] applied a time-dependent coupled HF method and consequently reported more accurate long-range interaction coefficients. van der Avoird et al. [33] reported a new potential (AWJ) by including these improved long-range coefficients and more basis sets. However, it was observed that the van der Waals well prediction of the potential was too shallow. This resulted in large discrepancies between the calculated second virial coefficient values and the experimentally observed results. Neglect of intramolecular electron correlation leading to significant short-range exchange repulsion in the intermolecular potential was identified and later confirmed to be the cause for this discrepancy. In response, they introduced two scaling constants to change the size and slope of the short-range exchange repulsion term to obtain a rescaled potential that yielded second virial coefficients that were in much better agreement with experiments.

Highly accurate experimental virial coefficient data sets were used by Stallcop et al. [6] to improve *ab initio* PES obtained as a result of calculations performed at the Coupled Cluster with Singles, Doubles and perturbative Triples CCSD(T) excitations level of theory with large basis sets. A semi-empirical relation between the parameters of the repulsive potential and the accurate virial coefficient data sets was also reported. Cappelletti et al. [7] also reported a potential which was an improvement of the AWJ potential, by firstly

computing *ab initio* PES at the CCSD(T) level of theory and then using accurate data from scattering, virial coefficients and other property measurements to improve the PES quality. An extensive *ab initio* study was conducted by Leonhard et al. [8] to develop not only an improved 2-body potential but also to analyze two 3-body potentials for their capability to reproduce thermodynamic properties if both the 2-body as well as 3-body potentials were used. The 2-body *ab initio* PES was rescaled to fit accurate second virial coefficient data. After comparison to experimental results, the 3-body potential due to Axilrod Teller (AT) [34] performed better than the one due to Stogryn [35], when used in combination with the 2-body potential.

Gomez et al.[36] reported an *ab initio* PES that was calculated using Symmetry-Adapted Perturbation Theory (SAPT). The accuracy of perturbative energies were compared against calculations at the CCSD(T) level of theory using large basis sets. They observed better agreement to experimental virial coefficients than previous unscaled PESs for the range of temperatures investigated. They attributed the consistently lower second virial coefficient predictions by using their PES, to possible overestimation of the van der Waals well within their calculations. Strąk et al. [37] also performed *ab initio* calculations at the CCSD(T) level of theory that resulted in a potential that was used in combination with molecular dynamics (MD) simulations to obtain an equation of state for the dimer. The resulting predictions of physical properties based on this equation of state were found to be in excellent agreement with experiments for a wide range of temperatures (up to 2000K) and pressures (up to 30GPa). Hellmann [9] recently performed *ab initio* calculations at the CCSD(T) level of theory using basis sets up to aug-cc-pV5Z supplemented with bond functions. The resulting 2-body (scaled) and 3-body potential was used to compute second and third (including 3-body effects) virial coefficients that were in better agreement with experiments than previously reported values. This is the potential applied in the present study. We go to lower temperatures than examined by Hellmann, applying PIMC methods for the nuclear quantum effects, which then allows us to ascertain the range of accuracy of the semi-classical approaches.

We have divided this paper into the following sections: various methods employed in this study are explained in Sec. II and subsections therein; Sec. III contains all the relevant computational details pertaining to different simulations performed; we present and discuss fully quantum virial coefficient results for molecular nitrogen in Sec. IV followed by concluding

statements in Sec. V.

II. METHODS

A. Semiclassical treatment of nuclear quantum effects

The semiclassical treatment of nuclear quantum effects using a given PES falls into the following two categories:

1. *Quantum corrections approach*

Expressions for the first-order quantum corrections to the second virial coefficient have been derived by Pack [38] for diatomic molecules under different conditions. These expressions have been obtained starting with the expansion of the quantum partition function in powers of $\hbar$ and then achieving a simplified expression by performing some of the integrations analytically (for further details, we point the interested reader to Ref. 38). For later reference, we note that Hellmann [9] used the expressions of Pack [38] for computing semiclassical second virial coefficients and derived for the first time, first-order quantum corrections to the third virial coefficient.

2. *Effective potential approach:*

One can also compute semiclassical virial coefficients by employing an effective potential (modified version of the given PES) based on the quadratic Feynman-Hibbs [39, 40] (QFH), Takahashi-Imada [41] (TI) or other similar methods. Within this effective potential approach, for instance, the QFH effective potential replaces the intermolecular pair potential U_2^{H} with the following form:

$$U_2^{\mathrm{QFH}} = U_2^H + \frac{\hbar^2\beta}{24m}\left[\boldsymbol{\nabla}^2 U_2^H + \frac{2}{r}\boldsymbol{\nabla} U_2^H\right]. \tag{3}$$

The effective potential obtained as a result can be imagined to make the atom more diffuse in nature as opposed to the classical case where the atoms are considered as point masses. For later reference, we note that we have used the QFH form of the effective potential in all our semiclassical virial coefficient calculations.

B. Path Integral Monte Carlo

Feynman's [39] discretized path integral (PI) formalism provides a route to incorporating nuclear quantum effects explicitly in virial coefficient calculations. Within this formalism, the quantum mechanical partition function of a system is mapped onto the classical partition function of a fictitious closed-ring polymer with P discretization points or 'beads'. When applied to a homonuclear diatomic, the expression for B_2 (and B_3 similarly) can be put in the form [25, 26]:

$$B_2(T) = -\frac{1}{2}\int d\mathbf{R}^{(1)}d\mathbf{b}^{(1)}d\mathbf{R}^{(2)}d\mathbf{b}^{(2)}\pi_{\mathbf{R}}(\mathbf{R}^{(1)})\pi_{\mathbf{R}}(\mathbf{R}^{(2)})\pi_{\mathbf{b}}(\mathbf{b}^{(1)})\pi_{\mathbf{b}}(\mathbf{b}^{(2)})f(\mathbf{R}^{(1)},\mathbf{b}^{(1)},\mathbf{R}^{(2)},\mathbf{b}^{(2)}). \tag{4a}$$

with the Mayer function given in terms of the intermolecular energy U averaged over all path-integral images:

$$f(\mathbf{R}^{(1)},\mathbf{b}^{(1)},\mathbf{R}^{(2)},\mathbf{b}^{(2)}) = e^{-\beta\bar{U}(\mathbf{R}^{(1)},\mathbf{b}^{(1)},\mathbf{R}^{(2)},\mathbf{b}^{(2)})} - 1, \tag{4b}$$

$$\bar{U}\left(\mathbf{R}^{(1)},\mathbf{b}^{(1)},\mathbf{R}^{(2)},\mathbf{b}^{(2)}\right) = \frac{1}{P}\sum_{i=0}^{P-1} U\left(\mathbf{R}_i^{(1)},\mathbf{b}_i^{(1)},\mathbf{R}_i^{(2)},\mathbf{b}_i^{(2)}\right). \tag{4c}$$

Here, $\mathbf{R}^{(n)}$ and $\mathbf{b}^{(n)}$ are the full set of position and orientation coordinates for all images of molecule n, such that the two atoms of the image i of molecule n are at $\mathbf{R}_i^{(n)} \pm \mathbf{b}_i^{(n)}/2$. As shown in Eq. 4a, the ideal-gas distributions of the image positions and orientations decouple, having the respective forms [26]:

$$\pi_{\mathbf{R}}(\mathbf{R}) = \left(\frac{P^{3/2}}{\Lambda_{2m}^3}\right)^P \exp\left[-\frac{\pi P}{\Lambda_{2m}^2}\sum_{i=0}^{P-1}|\mathbf{R}_{i+1}-\mathbf{R}_i|^2\right], \tag{5a}$$

$$\pi_{\mathbf{b}}(\mathbf{b}) = \frac{1}{Q_1}\exp\left[-\frac{\pi P}{\Lambda_{m/2}^2}\sum_{i=0}^{P-1}|\mathbf{b}_{i+1}-\mathbf{b}_i|^2\right] e^{-\beta\bar{u}(\mathbf{b})} \tag{5b}$$

where Q_1 is a normalization constant and $\bar{u}$ is the intramolecular (bond stretching) potential energy averaged over all images:

$$\bar{u}(\mathbf{b}) = \frac{1}{P}\sum_{i=0}^{P-1} u\left(b_i\right) \tag{5c}$$

with $b_i \equiv |\mathbf{b}_i|$; also in Eqs. 5a and 5b, $\Lambda_m = h/\sqrt{2\pi m k_{\mathrm{B}} T}$ is the thermal de Broglie wavelength for mass m. This decoupling allows positions and orientations to be sampled independently to generate configurations that can be accepted or rejected in a MC process that considers their coupling via the Mayer function $f(\mathbf{R}^{(1)},\mathbf{b}^{(1)},\mathbf{R}^{(2)},\mathbf{b}^{(2)})$.

C. Sampling of path-integral conformations for diatomic molecules

Presented below are some of the salient features of this orientation sampling algorithm which we have employed in this study. For additional details, we refer the interested reader to Ref. 26.

The $\mathbf{R}$ coordinates distributed as in Eq. 5a form a Gaussian ring, which can be sampled in sequence [19, 21, 42]. Starting from coordinate $\mathbf{R}_0$ at the origin, subsequent coordinates $\mathbf{R}_i$, $i = 1..P-1$, are sampled from a 3-dimensional Gaussian of standard deviation σ_i centered at $\mathbf{R}'_i$:

$$\sigma_i = \left(\frac{\Lambda_{2m}^2}{2\pi P} \frac{P+1-i}{P+2-i} \right)^{1/2}, \tag{6a}$$

$$\mathbf{R}'_i = \frac{P+1-i}{P+2-i} \mathbf{R}_{i-1}. \tag{6b}$$

Although the distribution of $\mathbf{b}$ coordinates in Eq. 5b have the same Gaussian form, they cannot be sampled directly due to the additional effect of the intramolecular potential $u(\mathbf{b})$, which for a rigid molecule has the effect of constraining the $\mathbf{b}$ to the surface of a sphere. Instead we sample according to an approximate distribution $\tilde{\pi}(\mathbf{b})$, constructed so it can be sampled directly, and correct for the approximation when deciding acceptance of the trial configuration.

More specifically, we use a bisection based algorithm to generate orientations for all the images of a ring in the following manner. At each stage, we are given two known orientations: $\{\mathbf{b}_i, \mathbf{b}_k\}$, and we seek to set the orientation of the image $\mathbf{b}_j$, $j = (i+k)/2$, according to $\tilde{\pi}(\mathbf{b})$, for the given $\{\mathbf{b}_i, \mathbf{b}_k\}$. Define the the angle $\psi_{ik} = \cos^{-1}(\mathbf{b}_i \cdot \mathbf{b}_k / b^2)$ and the bisector $\mathbf{a}_{ik} = (\mathbf{b}_i + \mathbf{b}_k)/2$. The new sample for $\mathbf{b}_j$ is given in terms of the polar and azimuthal angles, α_j and β_j respectively, defined with respect to the axis $\mathbf{a}_{ik}$. The angle β_j is chosen at random, uniformly on $[0, 2\pi]$, while α_j is given by the following, where C is chosen at random uniformly on [0,1]:

$$\alpha_j = \cos^{-1}\left[1 + (1/\kappa_{ik}) \ln\left(1 - C(1 - \exp[-2\kappa_{ik}])\right)\right], \tag{7a}$$

where

$$\kappa_{ik} = \frac{8P \cos(\psi_{ik}/2) \pi b^2}{(k-i)\Lambda_{m/2}^2}. \tag{7b}$$

The process begins by selecting the initial orientation $\mathbf{b}_0$ ($= \mathbf{b}_P$) at random uniformly on a sphere. Then, with $i = 0, k = P$ (and thus $\psi = 0$), the procedure above is used to determine

$\mathbf{b}_j$ for $j = P/2$. In the next step $\mathbf{b}_j$ is selected for $j = P/4$ ($i = 0, k = P/2$) and $3P/4$ ($i = P/2, k = P$), i.e., one between each pair of previously-placed adjacent vectors. The process is repeated until all image orientations have been chosen. The algorithm requires that P be of the form 2^n, for integer n. The $P/2$ orientations set in the final stage of the process are in fact sampled exactly from the target distribution $\pi_{\mathbf{b}}$ for the given $P/2$ orientations as placed by the preceding steps. The probability density for the resulting configuration is

$$\tilde{\pi}_{\mathbf{b}}(\mathbf{b}) = \prod_{\substack{l=1 \\ p=2^l}}^{n} \prod_{\substack{s=1,\text{odd} \\ j=sP/p \\ i,k=j\pm P/p}}^{p-1} \frac{\kappa_{ik} \exp[\kappa_{ik} \cos \alpha_j]}{2 \sinh \kappa_{ik}}, \tag{8}$$

This expression enters into Eq. 9 to determine the probability of accepting the new configuration:

$$P_{\text{acc}} = \min \left[1, \frac{\pi_{\mathbf{b}}(\mathbf{b}^{\text{new}})/\pi_{\mathbf{b}}(\mathbf{b}^{\text{old}})}{\tilde{\pi}_{\mathbf{b}}(\mathbf{b}^{\text{new}})/\tilde{\pi}_{\mathbf{b}}(\mathbf{b}^{\text{old}})} \frac{|f^{\text{new}}|}{|f^{\text{old}}|} \right] \tag{9}$$

where f^{new} and f^{old} are the Mayer function for the new and old coordinates, respectively; the absolute value is used because f may be negative. An analogous formula applies to the sampling of the $\mathbf{R}$ coordinates, but because the sampling distribution $\tilde{\pi}_{\mathbf{R}}$ equals $\pi_{\mathbf{R}}$, the π ratios cancel and the acceptance is based only on f. Sampling of the $\mathbf{R}$ and $\mathbf{b}$ coordinates is accomplished while holding the molecule centers fixed. Trials are also performed to sample the positions of the molecules with respect to each other.

D. PIMC with SemiClassical Beads (SCB)

Conventional PI treatments involve the use of classical beads (i.e., beads interacting via the unmodified potential) due to the use of the primitive approximation. However, many higher order propagators of the thermal density matrix have been shown to yield faster convergence and better precision in quantum calculations. These approaches have primarily been used to estimate the energy of various systems [41, 43–45]. Schenter [40] first applied the higher order Takahashi Imada (TI) propagator to obtain high quality semiclassical virial coefficients of water. We recently [46] extended this approach in PIMC calculations involving the helium atom and compared the performance of the TI propagator and a slightly modified Quadratic Feynman-Hibbs [39] (QFH) potential against the conventional classical-bead

results of Shaul et al. [19]. We showed that the use of higher order propagators resulted in a PI treatment where the corresponding beads of different rings experience a semiclassical potential as opposed to a classical potential.

For extension to the diatomic (or any multiatomic, for that matter), consider the working equations of the TI propagator in terms of $\mathcal{T}$ and $\mathcal{U}$ that denote the kinetic and potential energy operators of the Hamiltonian respectively:

$$\begin{aligned} Tr\left[e^{-\beta(\mathcal{T}+\mathcal{U})}\right] &= Tr\left[e^{-\frac{\beta}{P}\mathcal{T}}e^{-\frac{\beta}{P}\mathcal{U}'}\right]^P + O(\beta^5 P^{-4}), \\ \mathcal{U}' &= U + \frac{\hbar^2}{24m}\left(\frac{\beta}{P}\right)^2 \sum_{i=1}^{N} \left|\boldsymbol{\nabla}_i U\right|^2. \end{aligned} \tag{10}$$

Using the TI propagator (Eq. (10)) for PIMC calculations with semiclassical beads involves $\mathcal{U}'$ instead of U in Eq. (4c).

III. COMPUTATIONAL DETAILS

Mayer-sampling Monte Carlo (MSMC) [12] is used in all our virial coefficient calculations. Within each MSMC simulation, all types of MC trials that are part of the simulation are chosen with equal probability and the step sizes (where applicable) are decided based on running a short equilibration simulation. The samples are divided into 1000 blocks and different ratios as prescribed by MSMC are averaged within each of the blocks. The average and standard error of these ratios over all such blocks are computed. The final virial coefficient value is obtained by combining the different ratios as prescribed by MSMC while its standard deviation is computed based on standard errors of the ratios and error propagation formulas, properly accounting for correlation between the averages. We use a reference hard-sphere diameter of 4.5Å (same as Hellmann [9]) and perform our virial coefficient calculations over a set of 103 temperatures.

The *ab initio* potential (denoted as U_2^H) due to Hellmann [9] is used in our classical and semiclassical virial coefficient calculations, each computed using 10^9 configuration samples and two types of MC trials: 1) translation and 2) rotation of the dimer. We perform PIMC calculations using $P = 1$, 2, 4, 8, 16, 32 and (for B_2) 64 classical or semiclassical images (TI propagator) and collect 10^8 configuration samples each. Apart from the translation of the dimer, we also include MC trials to regrow the ring by translating the beads (see Sec. II C) and our recently developed orientation algorithm [26] (explained in Sec. II C).

We compute third virial coefficients for the same set of temperatures and numbers of beads that are used for B_2. We again use 10^9 samples, except for the PIMC calculations for which we use 10^8. We capture the non-additive interactions via the 3-body potential reported by Hellmann [9]. Also, we perform the semiclassical additive as well as non-additive simulations using the same QFH version of U_2^H as in Eq. (3).

IV. RESULTS AND DISCUSSION

A. Second virial coefficients

We perform classical virial coefficient calculations to reproduce the results of Hellmann in order to validate our implementation of the *ab initio* potential. In Fig. 1 we compare our classical results against Hellmann's and find excellent agreement for the entire range of temperatures.

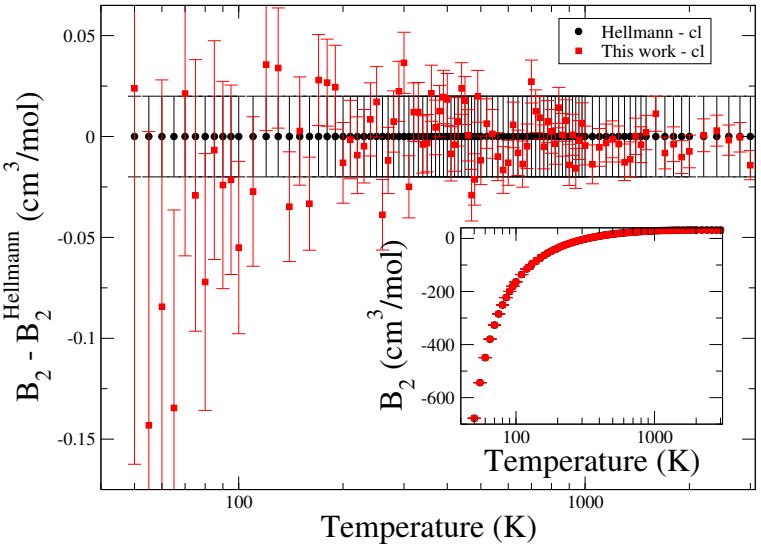

FIG. 1: Classical second virial coefficient (B_2) for N_2 comparing this work against Hellmann's [9]. Main plot shows the difference and inset plot shows the actual values. Error bars represent one standard deviation of the mean (68% confidence interval) for the components of the difference (i.e., not the uncertainties of the differences themselves, which would include both component uncertainties).

In Fig. 2 we compare our semiclassical second virial coefficient results against Hellmann's and observe excellent agreement for temperatures $T \geq 100$ K. The deviation observed for

lower temperatures can be explained by Hellmann's use of a different semiclassical approach (see Sec. II A): whereas we have used the effective potential approach based on the QFH version (Eq. (3)), Hellmann computed first order quantum corrections using the expressions derived by Pack [38]. Also, in the figure we present results for the TI effective potential (the 1-bead version of the PIMC with semiclassical beads, Eq. (10)). These results begin to deviate from the other semiclassical treatments at about 500 K, which is higher than the point where QFH and Hellmann's begin to differ. As we show below, comparison to more accurate PIMC results resolve this difference in favor of QFH/Hellmann results.

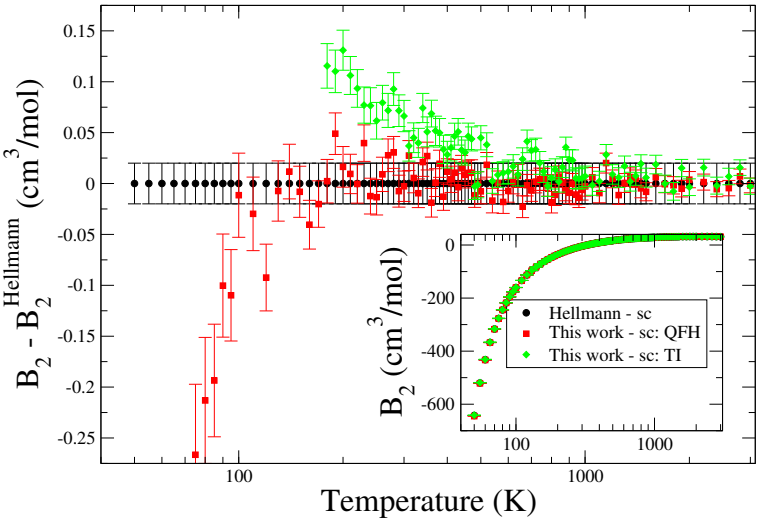

FIG. 2: Semiclassical second virial coefficient (B_2) for N_2 comparing this work against Hellmann's [9]. Main plot shows the difference and inset plot shows the actual values. Error bars represent one standard deviation of the mean (68% confidence interval) for the components of the difference. Low-temperature data for the main plot are off the bottom of the scale.

Figure 3 shows how the path-integral calculations converge with respect to the number of path-integral beads. We present results for both classical- and semiclassical-bead formulations. The figure shows that more beads are needed at lower temperatures, as expected, and in particular that below about 35 K eight or more beads are needed. For the obtained uncertainties, eight beads are needed at 35 K and the required number of beads doubles with every 5 K decrease in temperature. The figure also shows the approach using semiclassical beads offers a marginal advantage over the approach using classical beads – at conditions where the results are not converged in P the SCB-results are generally closer, but both approaches end up agreeing with the converged data at about the same P.

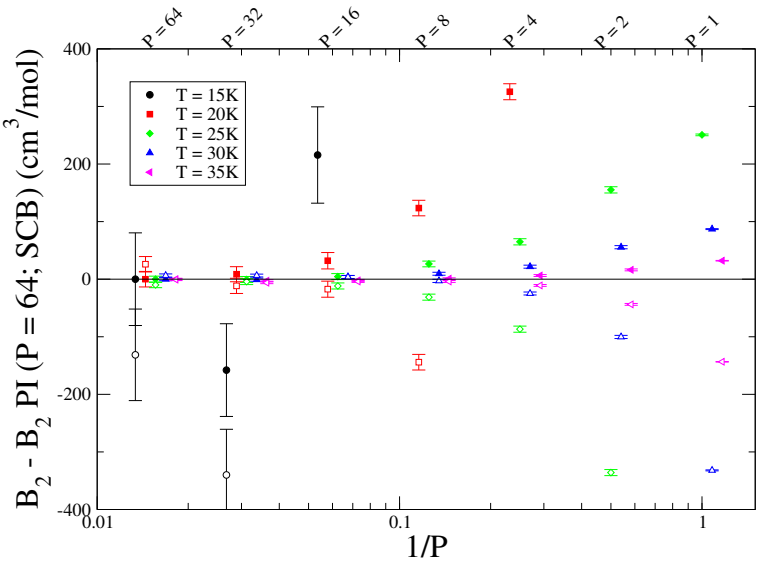

FIG. 3: Convergence of the second virial coefficient with respect to the number of path-integral beads. Plot presents the low-temperature values computed using PI-SCB (filled symbols) and conventional PI using classical beads (open symbols) for different values of P, differenced with respect to PI-SCB for $P = 64$. Values for 15 K for smaller P are off the scale. Some points are shifted slightly to the left or right for clarity. Error bars represent one standard deviation of the mean (68% confidence interval) for the components of the difference.

In Fig. 4 we plot the differences between the virial coefficients computed using the various approaches relative to the values computed using PI-SCB with $P = 64$ images. From this figure, we can see that there is good agreement between the experimental results and the various semiclassical and PIMC based approaches for conditions where experimental data are available for comparison ($T \geq 98$ K) – to some degree this is due to the large uncertainties in the experimental data at lower temperatures. The agreement with classical values deteriorates for temperatures less than ≈ 800 K (outside the range of the plot), indicating the onset of relevance of nuclear quantum effects. All semiclassical results become systematically too high below ≈ 250 K, with the TI treatment deviating the most and doing so up to ≈ 430 K. The present semiclassical approach and Hellmann's perform equally well over the range where they are accurate — the difference in these semiclassical approaches seen in Fig. 2 is not important because at these temperatures both are inaccurate.

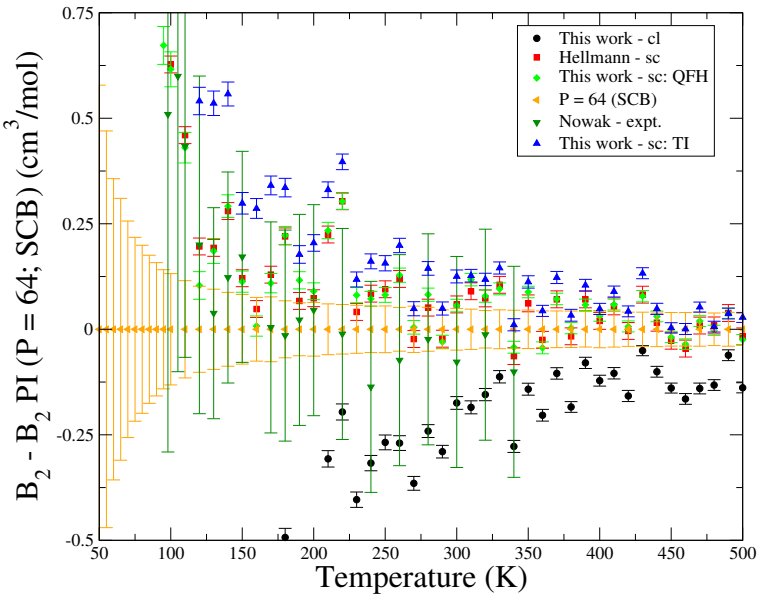

FIG. 4: Difference between second virial coefficients for N_2 determined using different approaches relative to the values computed using PI-SCB with $P = 64$ images. Experimental data are from Nowak et al. [47]; values for $T = 98$ and 105 K are differenced from interpolated PI-SCB values. Error bars represent one standard deviation of the mean (68% confidence interval) for the components of the difference.

B. Third virial coefficients

Figures 5 - 7 show results for B_3 corresponding to data presented in Figs. 1 - 3 for B_2, demonstrating qualitatively similar behavior. Figures 8 and 9 collect the key results showing the importance of nuclear quantum effects, and the (much more significant) multibody contributions to the potential. The computed values again have reasonable agreement with experiments, but are systematically lower. In Fig. 9 we show the same data to higher temperatures, but on an expanded scale and differenced with respect to our semiclassical data (which are more precise than the PI-SCB values used in Fig. 8). The precision of the calculation allows us to discern differences between the classical and semiclassical values over all temperatures shown. The semiclassical values generally agree with each other although QFH appears to have some advantage in showing better agreement with PIMC at lower temperatures, down to about 150 K.

The net impact of nuclear quantum effects on the pressure can be gauged by examining the scale of the difference plots — Figs. 4 and 8 — with the scale of full values given by the

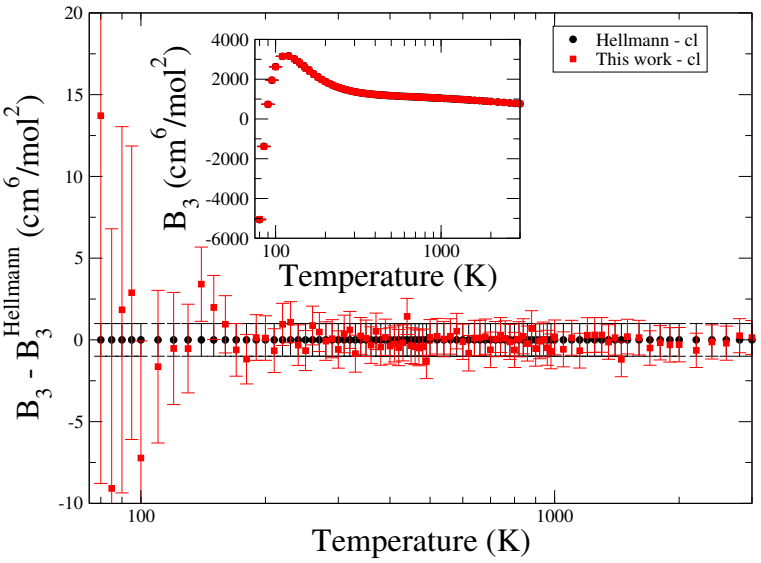

FIG. 5: Same as Fig. 1 except showing the third virial coefficient (B_3).

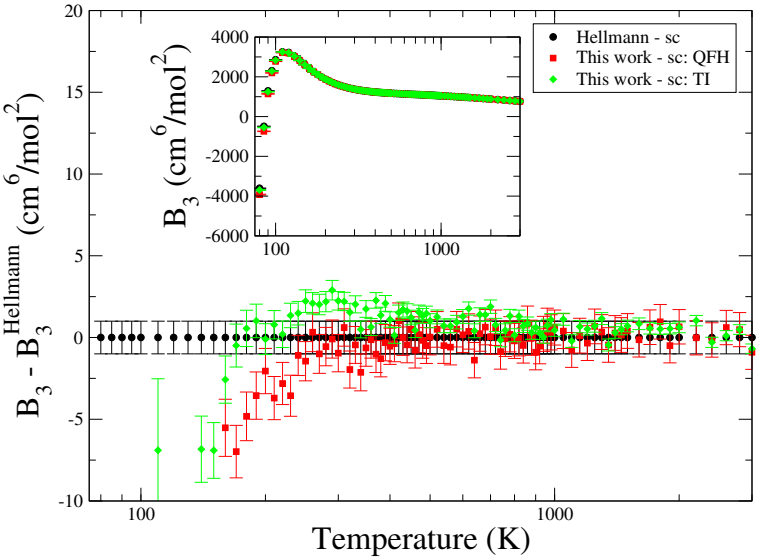

FIG. 6: Same as Fig. 2 except showing the third virial coefficient (B_3).

insets of Figs. 2 and 6, for B_2 and B_3, respectively. Except at low temperatures ($T <$ 60 K), the correction to the classical B_2 is about a percent or less, and for B_3 the effect is less than half a percent for most temperatures above 100 K. The overall effect depends on density, of course, but for most conditions above the critical temperature (126.2 K), nuclear quantum effects alter the non-ideal contribution to the pressure by about a percent or less, and thus the pressure itself by even less. Nevertheless, the effects are measurable, and must be accounted for when trying to reproduce experimental virial coefficients. We note that, in

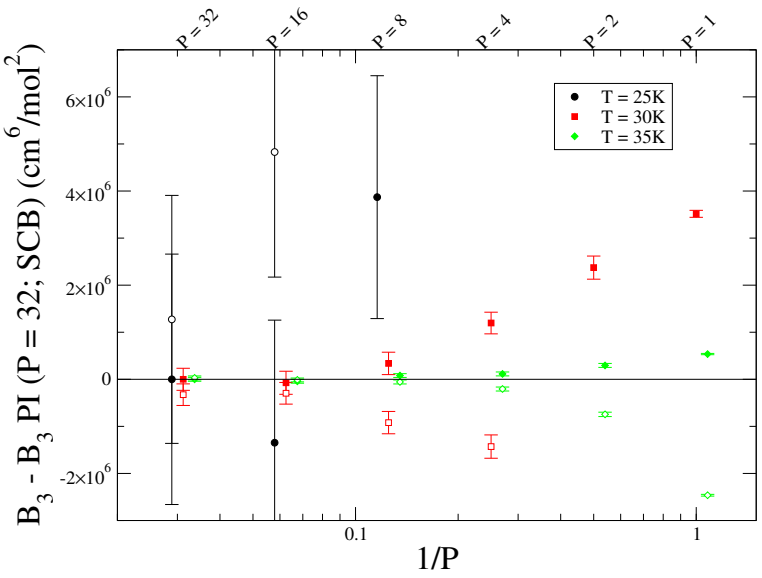

FIG. 7: Same as Fig. 3 except showing the third virial coefficient (B_3).

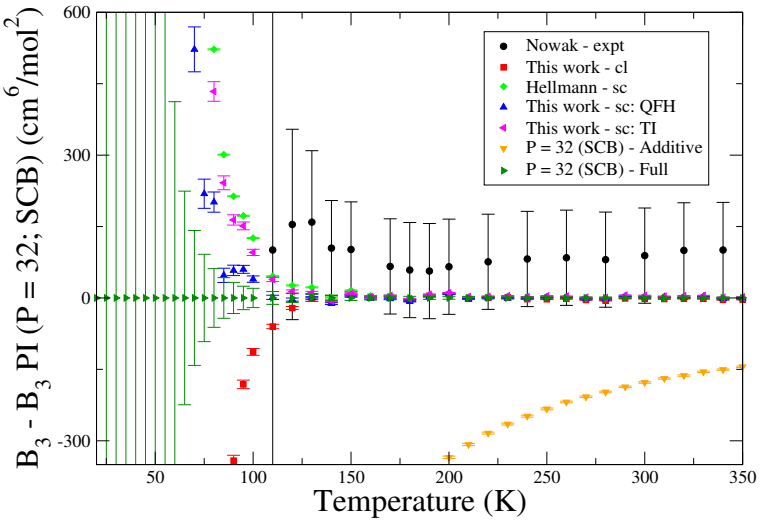

FIG. 8: Same as Fig. 4 except showing the third virial coefficient (B_3).

comparison, the effect on B_3 of non-additivity of the potential about ten times larger than the nuclear quantum effects, and exceeds 1% of the total B_3 for all temperatures.

All virial coefficient values are provided in the supplementary material.

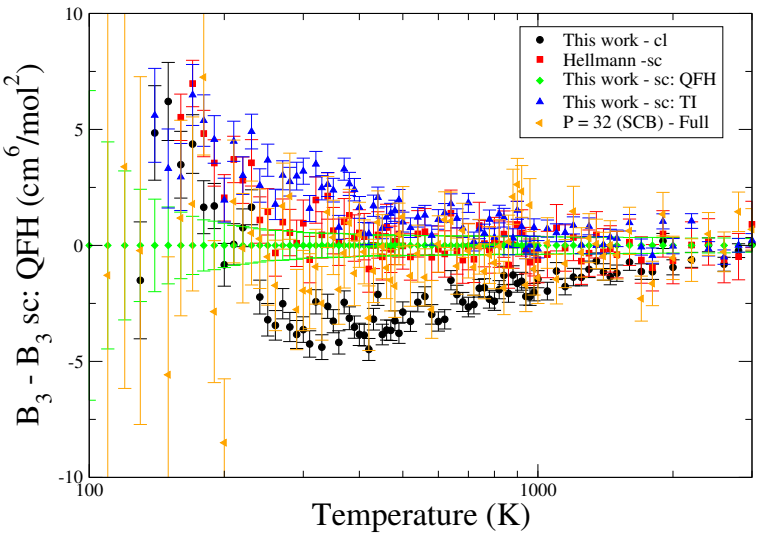

FIG. 9: Same as Fig. 8 except differenced relative to semiclassical results computed in this work rather than PI-SCB.

V. CONCLUSION

We have calculated fully quantum virial coefficients for molecular nitrogen by explicitly including nuclear quantum effects via the PIMC method considering both classical and semiclassical beads, finding the latter to be marginally better. We have also employed an algorithm that we recently [26] developed to sample orientations of diatomic molecules, in all our PIMC calculations. We have compared our PIMC results against experimental data available in literature and find them in good agreement at high temperature. At low temperatures, systematic deviations emerge, but are small relative to the experimental uncertainties. The results show the importance of handling nuclear quantum effects using at least semiclassical approaches when computing precise virial coefficients.

Extension of the direct-sampling methodology used here to more complex molecules — multiatomics and/or molecules with flexibility — is not straightforward, and will require some additional development. We expect that translation and rotation will still separate cleanly, and that rigid linear multiatomics will be tractable with minor extension of the present formulation. For nonlinear molecules, two orientation vectors must be specified for each molecule image, and there is additional complication from the differing masses of the atoms. We think a bisection approach can still be applied, with selection of each image orientation based only on the orientations of the two images adjacent to it, as set in the

preceding iteration. It is unlikely that the last-stage distribution can be solved exactly as was done for the rigid diatomic, but only an approximation is needed, and this should be obtainable. Flexibility adds a different set of problems. Semi-rigid molecules should be handled by treating orientation sampling separate from conformational sampling, but apart from this we have not yet attempted a general prescription for this case.

VI. ACKNOWLEDGMENTS

We sincerely thank Dr. Robert Hellmann for helping us implement the 2-body and 3-body PESs correctly. Computational resources were provided by UB's Center for Computational Research (CCR). This work is supported by the U.S. National Science Foundation through Grants CHE-1027963 and CBET-1510017.

VII. REFERENCES

[1] J. Mayer and M. Mayer, *Statistical Mechanics* (Wiley, New York, New York, 1977).

[2] E. Mason and T. Spurling, *The Virial Equation of State* (Pergamon Press, Oxford, 1969).

[3] J. P. Hansen and I. R. McDonald, *Theory of Simple Liquids*, 3 edition (Academic Press, 2006).

[4] P. E. S. Wormer and A. van der Avoird, J. Chem. Phys. **81** (4), 1929 (1984).

[5] V. Aquilanti, D. Ascenzi, M. Bartolomei, D. Cappelletti, S. Cavalli, M. de Castro Vitores and F. Pirani, J. Am. Chem. Soc. **121** (46), 10794 (1999).

[6] J. R. Stallcop and H. Partridge, Chem. Phys. Lett. **281** (1 – 3), 212 (1997).

[7] D. Cappelletti, F. Vecchiocattivi, F. Pirani, E. L. Heck and A. S. Dickinson, Mol. Phys. **93** (3), 485 (1998).

[8] K. Leonhard and U. K. Deiters, Mol. Phys. **100** (15), 2571 (2002).

[9] R. Hellmann, Mol. Phys. **111** (3), 387 (2013).

[10] A. J. Masters, J. Phys.: Condens. Matter **20**, 283102 (2008).

[11] G. P. Lepage, J. Comput. Phys. **27** (2), 192 (1972).

[12] J. K. Singh and D. A. Kofke, Phys. Rev. Lett. **92** (22), 220601 (2004).

[13] R. Bukowski, K. Szalewicz, G. C. Groenenboom and A. van der Avoird, J. Chem. Phys. **128** (9), 094314 (2008).

[14] K. Szalewicz, C. Leforestier and A. van der Avoird, Chem. Phys. Lett. **482**, 1 (2009).

[15] G. Garberoglio and A. H. Harvey, J. Res. Natl. Inst. Stand. Technol. **114** (5), 249 (2009).

[16] G. Garberoglio and A. H. Harvey, J. Chem. Phys. **134** (13), 134106 (2011).

[17] G. Garberoglio, M. R. Moldover and A. H. Harvey, J. Res. Natl. Inst. Stand. Technol. **116** (4), 729 (2011).

[18] G. Garberoglio, Chem. Phys. Lett. **525-526**, 19 (2012).

[19] K. R. Shaul, A. J. Schultz and D. A. Kofke, J. Chem. Phys. **137** (18), 184101 (2012).

[20] K. R. S. Shaul, A. J. Schultz, D. A. Kofke and M. R. Moldover, Chem. Phys. Lett. **531**, 11 (2012).

[21] K. Patkowski, W. Cencek, P. Jankowski, K. Szalewicz, J. B. Mehl, G. Garberoglio and A. H. Harvey, J. Chem. Phys. **129** (9), 094304 (2008).

[22] G. Garberoglio and J. K. Johnson, ACS Nano **4** (3), 1703 (2010).

[23] G. Garberoglio, P. Jankowski, K. Szalewicz and A. H. Harvey, J. Chem. Phys. **137** (15), 154308 (2012).

[24] G. Garberoglio, Chem. Phys. Lett. **557**, 26 (2013).

[25] G. Garberoglio, P. Jankowski, K. Szalewicz and A. H. Harvey, J. Chem. Phys. **141** (4), 044119 (2014).

[26] R. Subramanian, A. J. Schultz and D. A. Kofke, J. Chem. Phys. submitted (2016).

[27] T. Cui, E. Cheng, B. Alder and K. Whaley, Phys. Rev. B **55** (18), 12253 (1997).

[28] R. M. Berns and A. van der Avoird, J. Chem. Phys. **72**, 6107 (1980).

[29] F. Mulder, G. V. Dijk and A. V. D. Avoird, Mol. Phys. **39** (2), 407 (1980).

[30] T. Luty, A. van der Avoird and R. M. Berns, J. Chem. Phys. **73** (10), 5305 (1980).

[31] C. Nyeland, J. Phys. Chem. **88** (6), 1216 (1984).

[32] F. Visser, P. E. S. Wormer and P. Stam, J. Chem. Phys. **79** (10), 4973 (1983).

[33] A. van der Avoird, P. E. S. Wormer and A. P. J. Jansen, J. Chem. Phys. **84**, 1629 (1986).

[34] B. M. Axilrod and E. Teller, J. Chem. Phys. **11** (6), 299 (1943).

[35] D. E. Stogryn, J. Chem. Phys. **50** (11), 4967 (1969).

[36] L. Gomez, B. Bussery-Honvault, T. Cauchy, M. Bartolomei, D. Cappelletti and F. Pirani, Chem. Phys. Lett. **445** (4 – 6), 99 (2007).

[37] P. Strąk and S. Krukowski, J. Chem. Phys. **126** (19), 194501 (2007).

[38] R. T. Pack, J. Chem. Phys. **78** (12), 7217 (1983).

[39] R. P. Feynman and A. R. Hibbs, *Quantum Mechanics and Path Integrals*, 1 edition (McGraw-Hill Companies, Inc., New York, 1965), emended by Daniel F. Styer.

[40] G. K. Schenter, J. Chem. Phys. **117** (14), 6573 (2002).

[41] M. Takahashi and M. Imada, J. Phys. Soc. Jpn. **53** (11), 3765 (1984).

[42] L. D. Fosdick and H. F. Jordan, Phys. Rev. **143** (1), 58 (1966).

[43] W. Janke and T. Sauer, Phys. Lett. A **165** (3), 199 (1992).

[44] M. Suzuki, Phys. Lett. A **201**, 425 (1995).

[45] T. M. Yamamoto, J. Chem. Phys. **123** (10), 104101 (2005).

[46] R. Subramanian, A. J. Schultz and D. A. Kofke, in *Foundations of Molecular Modeling and Simulation: Select Papers from FOMMS 2015* (R. Q. Snurr, C. S. Adjiman and D. A. Kofke, eds.), chapter 6, 93–106 (Springer Singapore, Singapore, 2016).

[47] P. Nowak, R. Kleinrahm and W. Wagner, J. Chem. Thermodyn. **29** (10), 1137 (1997).